Geographia Technica, Vol. 22, Issue 1, 2027, pp 106 to 119

CLOUD-BASED MULTI-TEMPORAL SAR-OPTICAL FUSION USING RANDOM FOREST FOR GEOSPATIAL INTELLIGENCE MONITORING OF KIPP IKN NUSANTARA

Fajar Sidik SUGANDA [1*] **& *Asep Adang SUPRIYADI*** [1]

DOI: 10.21163/GT_2027.221.08

ABSTRACT

The development of Indonesia's new capital (IKN) Nusantara drives dramatic land-cover transformation across a strategic 17,599-hectare area under the persistent cloud cover of Kalimantan, where optical remote sensing alone is insufficient for continuous monitoring. This study proposes a cloud-based multi-temporal SAR-optical fusion approach using Random Forest classification for geospatial-intelligence (GEOINT) monitoring of the Core Government Area (KIPP) of IKN. Using Google Earth Engine, we processed 70 Sentinel-1 GRD and 52 Sentinel-2 images for 2022 and 61 and 81 images for 2024, building a 12-band fusion stack (SAR backscatter VV, VH, VV/VH; optical B2, B3, B4, B8, B11, B12; and NDVI, NDBI, NDWI). Six experiments compared SAR-only, optical-only, and fusion configurations. The Random Forest fusion achieved 88.89% overall accuracy and 0.8609 kappa for 2022 and 85.12% and 0.8127 for 2024 (assessed against ESA WorldCover 2021 class definitions; see Section 2.7), outperforming SAR-only (63.20%) and optical-only (86.44%). Change detection revealed 899.64 ha of direct vegetation-to-built-up conversion, a 60% expansion of built-up area driven by IKN construction. This is the first cloud-based multi-temporal fusion framework applied to KIPP IKN monitoring, with implications for spatial planning, security surveillance, and environmental compliance.

Keywords: *sar-optical fusion; random forest; Google Earth Engine; geospatial intelligence; IKN Nusantara.*

1. INTRODUCTION

Land use and land cover (LULC) classification using satellite remote sensing is an indispensable tool for monitoring environmental change, urban expansion, and infrastructure development (Pande et al., 2024), (Fitri et al., 2025). Free Sentinel-1 SAR and Sentinel-2 imagery, combined with cloud platforms such as Google Earth Engine (GEE), has democratized large-scale geospatial analysis (Latif et al., 2025). The Random Forest (RF) algorithm performs robustly in LULC mapping through its handling of high-dimensional features and resistance to overfitting (Dagne et al., 2023), (Al-Dousari et al., 2023), and fusing complementary SAR and optical information improves accuracy over single-modality approaches by combining SAR's all-weather capability with optical's spectral richness (Irfan et al., 2025), (Y. Li & Xiao, 2025). State-of-the-art Sentinel-2 classification reports 75-85% accuracy regionally, with multi-temporal analysis increasingly critical for capturing dynamic landscapes (Jocea et al., 2025).

Geospatial intelligence (GEOINT) is the exploitation and analysis of imagery and geospatial information to describe, assess and visually depict physical features and geographically referenced activities on the Earth in support of decision-making (Yusfan et al., 2021; Djati & Gunawan, 2025). In this study GEOINT refers to the use of multi-temporal land-cover change over a strategic national asset the KIPP of IKN to derive indicators for spatial-planning verification and security-perimeter monitoring. Despite these advances, several gaps remain in applying SAR-optical fusion to rapidly transforming strategic infrastructure in tropical regions.

----

[1] *Sensing Technology Study Program, Faculty of Defense Science and Technology, Republic of Indonesia Defense University, Sentul, West Java, Indonesia.* [*] *Corresponding author: fajarsidiksugandaa@gmail.com (FJS); aadangsupriyadi@gmail.com (AAS).*

First, fusion has mostly been demonstrated in temperate or sub-tropical contexts; its generalizability to tropical Indonesian landscapes with persistent cloud cover (often 60-80% year-round) is underexplored.

Second, change-detection studies typically address long-term decadal analysis (Jagannathan et al., 2025), yet megaproject construction produces major change within 2-3 years, requiring shorter-interval frameworks that are seldom evaluated. Third, comprehensive fusion-based monitoring of the Core Government Area (KIPP) of Indonesia's new capital (IKN)-the largest greenfield capital relocation in modern history-has not been published. Fourth, while urban built-up change detection exists (Feng et al., 2021), frameworks designed specifically for geospatial-intelligence (GEOINT) applications on strategic national infrastructure are absent for Indonesian contexts (Yusfan et al., 2021), (Djati & Gunawan, 2025), (Yusuf Samad et al., 2023).

Filling these gaps is urgent: during 2022-2024 KIPP IKN underwent intensive construction-Istana Garuda, Sumbu Kebangsaan, and Kemenko-transforming roughly 17,000 ha of Kalimantan rainforest and demanding evidence-based monitoring (Cholidah et al., 2024). This study proposes a cloud-based multi-temporal SAR-optical fusion framework using Random Forest for GEOINT monitoring of KIPP IKN, processed entirely in Google Earth Engine. Its objectives are: (1) to develop a 12-band SAR-optical fusion stack and evaluate Random Forest performance against single-modality baselines across two timeframes; (2) to quantify 2022-2024 land-cover transitions revealing GEOINT-relevant urban-transformation patterns; (3) to provide an actionable monitoring framework supporting spatial planning and security surveillance for similar strategic areas (Adi et al., 2025).

2. MATERIALS AND METHODS

2.1. Study Area

The study area is the Kawasan Inti Pusat Pemerintahan (KIPP) of Ibu Kota Nusantara (IKN), in Sepaku Subdistrict, Penajam Paser Utara Regency, East Kalimantan (**Fig. 1**). A bounding box of ~17,599 ha (116.650-116.780 E, 1.030-0.920 S) encompasses the 6,671-ha official KIPP boundary and its immediate context, including Pemaluan, Bumi Harapan, and Bukit Raya villages. This tropical-rainforest landscape has transformed rapidly since IKN construction began in 2022, with landmarks such as Istana Garuda and the Sumbu Kebangsaan boulevard built within the study period.

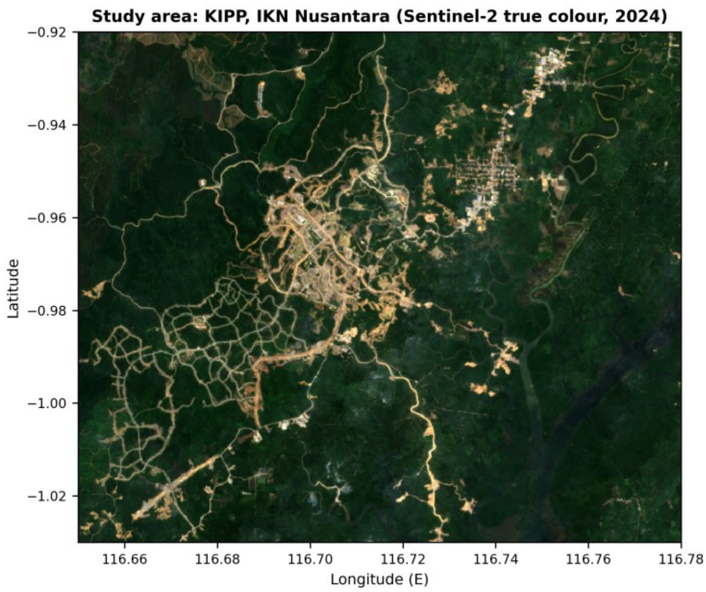

Fig. 1. Study area showing the Kawasan Inti Pusat Pemerintahan (KIPP) of Indonesia's new capital city (IKN) Nusantara.

2.2. Data Acquisition

Two complementary imagery sources were accessed through Google Earth Engine (**Fig. 2**) (Nigar et al., 2024). Sentinel-1 SAR Ground Range Detected (GRD) imagery was acquired in Interferometric Wide swath mode, descending orbit, dual polarization (VV, VH), yielding 70 images for 2022 and 61 for 2024, consistent with multi-temporal SAR monitoring for Indonesian contexts (Aldiansyah et al., 2024). Sentinel-2 Surface Reflectance Harmonized imagery filtered to <60% cloud cover yielded 52 images for 2022 and 81 for 2024. ESA WorldCover v200 (10 m, 2021) provided ground reference as pseudo-labels, remapped to five classes: built-up (0), bare land (1), vegetation (2), cropland (3), and water (4) (Carneiro et al., 2025). Both collections were filtered to the study-area boundary with GEE's filterBounds and filterDate.

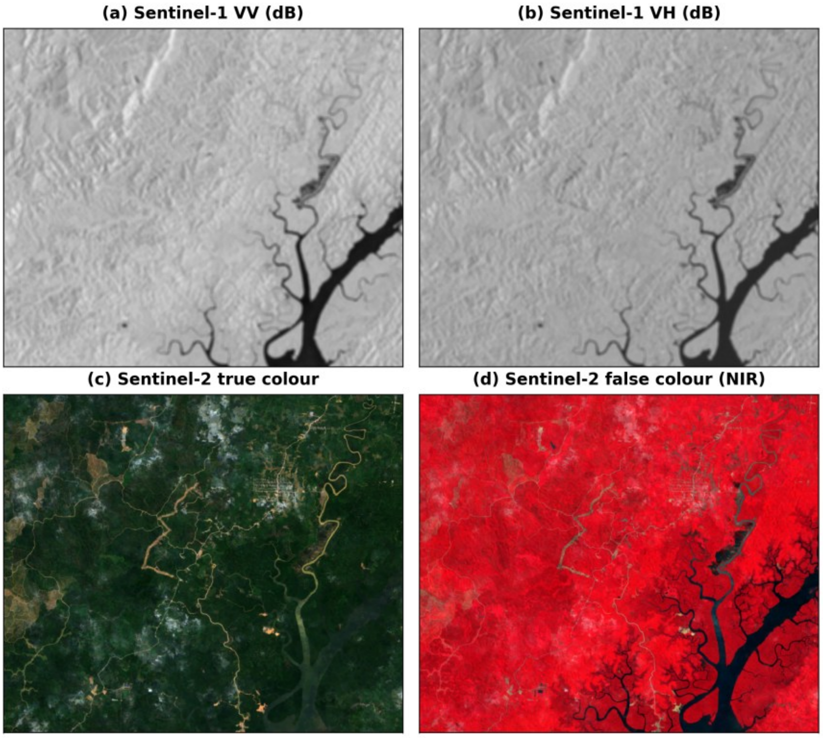

Fig. 2. Sample multi-modal input data over the KIPP IKN study area.

The cloud-based strategy retrieved a comprehensive multi-temporal dataset (**Table 1**): 70 and 61 Sentinel-1 GRD images and 52 and 81 Sentinel-2 SR images for 2022 and 2024 respectively (60% cloud threshold), over a 17,599.25-ha area confirmed by GEE's pixelArea reducer, encompassing the 6,671-ha KIPP boundary plus surrounding context.

Table 1.

Multi-temporal satellite imagery acquisition summary.

Parameter	2022 (baseline)	2024 (current)	Specification
Sentinel-1 GRD images	70	61	IW mode, descending
Sentinel-2 SR images	52	81	Cloud cover < 60%
S1 polarization	VV + VH	VV + VH	Plus VV/VH ratio
S2 spectral bands	6 bands	6 bands	B2, B3, B4, B8, B11, B12
S2 cloud masking	QA60	QA60	Bits 10 & 11
ROI total area	17,599.25 ha	17,599.25 ha	Bounding box

2.3. Preprocessing and Fusion Stack Construction

Sentinel-1 imagery was provided as backscatter in decibels following ESA's standard processing (thermal-noise removal, radiometric calibration, terrain correction). A 3x3 focal-mean filter was applied to the median composite for speckle reduction, and a VV/VH ratio band (VV.divide(VH)) was added to enhance textural discrimination. Sentinel-2 imagery was cloud- and cirrus-masked using the QA60 band (bits 10-11), then median-composited into a cloud-free annual composite. The optical composite comprised six bands (B2, B3, B4, B8, B11, B12) plus three normalized-difference indices (Aos & Putri, 2023): NDVI = (B8-B4)/(B8+B4), NDBI = (B11-B8)/(B11+B8), and NDWI = (B3-B8)/(B3+B8). The final fusion stack comprised 12 bands integrating SAR (3) and optical (9) information per period. In this study, "multi-temporal" denotes the two annual epochs (2022 and 2024) used for post-classification change detection, not intra-annual seasonal compositing: for each epoch every cloud-masked scene of the calendar year was reduced to a single per-pixel median composite. Seasonal (e.g. quarterly) sub-composites were not constructed because the persistent cloud cover over KIPP IKN leaves too few clear observations per quarter for a stable median, whereas an annual median maximises the number of valid observations per pixel.

2.4. Training Sample Generation

To ensure spatially representative samples with minimal manual labelling, stratified random sampling was applied to the ESA WorldCover label image, following auxiliary-data integration in heterogeneous-landscape classification (Shandu et al., 2026). GEE's stratifiedSample generated 5,000 points (1,000 per class; seed 42), partitioned into training (70%), validation (15%), and testing (15%). After feature extraction at 10 m, the final dataset comprised 3,528 training, 779 validation, and 693 testing points. ESA WorldCover 2021 is used solely to locate the stratified sample points; it is not used as a wall-to-wall validation layer or overlaid on the classified maps.

The stratified sampling produced 5,000 points across five classes (**Table 2**). The distribution is extremely imbalanced, typical of pristine rainforest: vegetation dominated at 92.1% (16,287.95 ha) while built-up was merely 0.2% (35.81 ha), confirming KIPP as effectively greenfield before construction.

Table 2.

Class distribution in study area (2021 ESA WorldCover baseline).

Class	Code	Area (ha)	Percentage	Sample Points
Vegetation	2	16,287.95	92.1%	1,000
Water body	4	774.86	4.4%	1,000
Bare land	1	336.12	1.9%	1,000
Cropland	3	164.51	0.9%	1,000
Built-up	0	35.81	0.2%	1,000
Total	-	17,599.25	100%	5,000

2.5. Random Forest Classification

The Random Forest (RF) algorithm was used for its robustness against overfitting, capacity for high-dimensional features, and proven superiority over tree-based alternatives such as CART for Sentinel-2 imagery (Gulci et al., 2025), (Syaban & Appiah-Opoku, 2024), (Kasahun & Legesse, 2024). Six experiments evaluated each modality's contribution:

RF SAR-only 2022 (3 bands: VV, VH, ratio)
RF Optical-only 2022 (9 bands: 6 spectral + 3 indices)
RF Fusion 2022 (12 bands combined) Proposed
RF SAR-only 2024
RF Optical-only 2024
RF Fusion 2024 - Proposed

The classifier was implemented using GEE's ee.Classifier.smileRandomForest with 100 trees and default hyperparameters for other settings, a configuration validated in recent multi-temporal Sentinel land cover studies (Lemenkova, 2025). Training was performed using the 70% split, with each pixel feature vector treated as an independent sample.

2.6. Multi-temporal Change Detection

Post-classification change detection encoded pairwise transitions between the two periods. A 5x5 transition matrix was built by computing pixel-wise area for every from-to class combination using GEE's ee.Image.pixelArea()-robust for tropical regions where cloud cover challenges single-date analyses. GEOINT-relevant transitions were flagged: vegetation-to-built-up (direct deforestation), bare-to-built-up (completed construction), and vegetation-to-bare (pre-construction clearing). Classified and change maps were exported as GeoTIFFs in EPSG:32750 at 10 m.

2.7. Accuracy Assessment

Accuracy was assessed from the error matrix: Overall Accuracy (OA), Cohen's Kappa, and per-class Producer's and User's Accuracy, computed independently for each of the six configurations on the held-out 15% test subset (Rangel et al., 2025). Both epochs are trained and tested against the same ESA WorldCover 2021 label set; the 2024 sample points were not re-labelled. Because the 2024 imagery post-dates the reference by three years, the 2024 accuracy is therefore assessed against 2021-vintage class definitions and carries label noise on the ~9% of the study area that genuinely changed land cover in the interim (Section 3.5). The 2024 figures should be read relative to the WorldCover-2021 definition rather than as a strict like-for-like comparison with 2022, whereas the one-year offset makes this effect negligible for 2022. A reference-independent check of the 2024 result against Dynamic World, which does not use ESA WorldCover, is reported in Section 3.4.1.

3. RESULTS

3.1. Random Forest Classification Performance

The six experiments consistently supported the hypothesis that SAR-optical fusion outperforms single-modality approaches (**Table 3**). For 2022, RF Fusion achieved 88.89% OA and 0.8609 Kappa-a 2.45-point improvement over optical-only (86.44%, kappa=0.8303) and 25.69 points over SAR-only (63.20%, kappa=0.5399); a McNemar test confirmed the fusion-over-optical gain was significant (chi2=4.83, p=0.028). For 2024 the hierarchy held-Fusion 85.12% OA, 0.8127 Kappa, versus optical-only (83.68%, kappa=0.7949) and SAR-only (62.40%, kappa=0.5286)-but the fusion-over-optical gain was smaller and not significant (chi2=1.69, p=0.19), indicating that SAR's principal benefit under rapidly changing conditions is robustness rather than a large accuracy margin. The modest 3.77-point decline from 2022 to 2024 reflects the mismatch between the 2021 labels and the evolving 2024 landscape.

Table 3.

Random Forest classification performance across modalities and periods.

Method	2022 OA (%)	2022 Kappa	2024 OA (%)	2024 Kappa
RF SAR-only	63.20	0.5399	62.40	0.5286
RF Optical-only	86.44	0.8303	83.68	0.7949
RF Fusion (proposed)	88.89	0.8609	85.12	0.8127
Δ (Fusion vs Optical)	+2.45	+0.0306	+1.44	+0.0179
Δ (Fusion vs SAR)	+25.69	+0.3210	+22.72	+0.2842

Because the held-out test set is class-balanced (~139 points per class), the overall accuracy is essentially the mean of the five per-class accuracies; the modest aggregate gain therefore averages one large improvement against three near-flat classes (**Table 4**). The optical-to-fusion gain is concentrated in built-up (Producer's Accuracy +6.7 percentage points in 2022) and cropland (+7.1 points in 2024) the transition classes central to GEOINT monitoring because SAR backscatter (double-bounce from vertical structures, textural separation of cropland from bare soil) adds information exactly where the optical signal is ambiguous, whereas vegetation and water are already near-ceiling with the NDVI and NDWI indices. By 2024 built-up is spectrally mature and its fusion gain disappears, shifting SAR's marginal value to cropland and vegetation.

Table 4.

Per-class change in Producer's and User's Accuracy from optical-only to fusion (percentage points; negative = fusion lower).

Class	ΔPA 2022	ΔUA 2022	ΔPA 2024	ΔUA 2024
Built-up	+6.7	+1.6	−1.2	+1.6
Bare land	+0.0	+3.5	−0.7	−0.2
Vegetation	+0.8	+5.6	+0.8	+5.4
Cropland	+3.7	+2.6	+7.1	+2.8
Water	+0.7	−0.6	+0.6	−1.5

3.2. Per-Class Performance Analysis (Confusion Matrix)

The confusion matrix for the RF Fusion 2022 model (**Table 5**) reveals strong diagonal dominance across all five classes. Vegetation achieved the highest classification accuracy (122/130 = 93.8% Producer's Accuracy), followed closely by water bodies (140/150 = 93.3%) and built-up (135/149 = 90.6%). Cropland reached 84.3% (113/134), while bare land was the most challenging class at 81.5% (106/130), owing to its spectral overlap with both built-up and vegetation during active construction. The uniformly high per-class accuracies all exceeding 81% indicate that the SAR-optical fusion stack discriminates the five land-cover types reliably even amid the landscape heterogeneity of KIPP IKN.

Table 5.

Confusion matrix for RF Fusion 2022 classification (test set, n=693).

Actual / Predicted	Built-up	Bare	Vegetation	Cropland	Water
Built-up (n=149)	135	11	3	0	0
Bare land (n=130)	17	106	2	5	0
Vegetation (n=130)	4	0	122	2	2
Cropland (n=134)	4	9	2	113	6
Water (n=150)	0	5	0	5	140

The full classification maps reveal the spatial distribution of land cover transformation across the KIPP IKN study area for both periods (**Fig. 3**). The 2024 map (panel b) demonstrates substantially expanded built-up coverage (red), particularly concentrated in the central area corresponding to the core development zone of IKN.

3.3. Multi-temporal Land Cover Distribution

Application of the trained RF Fusion classifiers to the full 17,599-hectare study area revealed dramatic land cover transformation between 2022 and 2024 (**Table 6**). Built-up area exhibited a striking increase, expanding from 785.35 hectares in 2022 to 1,258.83 hectares in 2024 an absolute increase of 473.48 hectares representing a 60.3% expansion within two years. Even more pronounced in relative terms, bare land expanded from 151.32 to 717.06 hectares (+373.9%), reflecting extensive land clearing that constitutes a pre-construction pipeline.

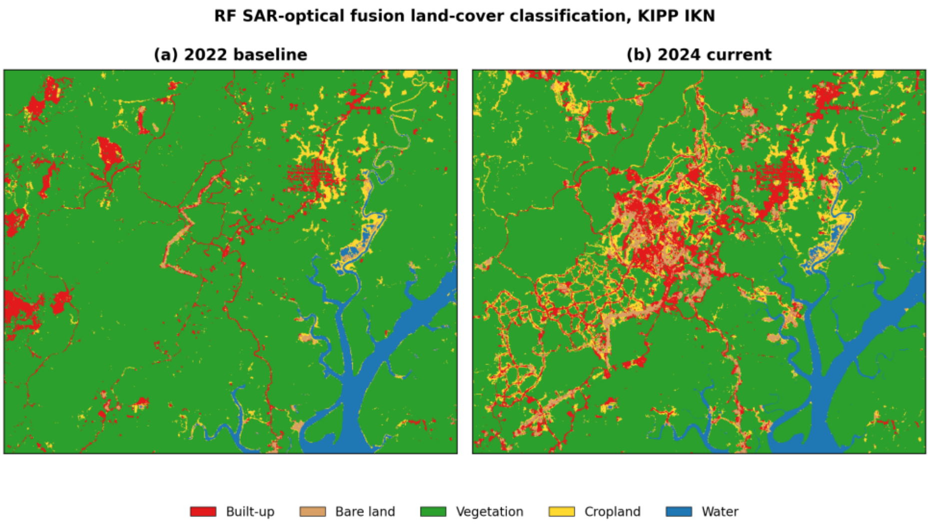

Fig. 3. Multi-temporal land cover classification maps showing (a) 2022 baseline and (b) 2024 current period.

Cropland nearly doubled (+99.0%, 630.48 → 1,254.96 ha), likely reflecting agricultural intensification by displaced communities, while vegetation declined by 1,660.04 hectares (10.9% reduction) as forest was progressively converted. Water bodies remained essentially stable (−0.4%), consistent with the absence of major impoundment within the core zone during this period.

Table 6.

Multi-temporal land cover distribution (hectares).

Class	2022 (ha)	2024 (ha)	Change (ha)	Change (%)
Built-up	785.35	1,258.83	+473.48	+60.3%
Bare land	151.32	717.06	+565.73	+373.9%
Vegetation	15,175.45	13,515.40	-1,660.04	-10.9%
Cropland	630.48	1,254.96	+624.48	+99.0%
Water	856.65	852.99	-3.65	-0.4%

3.4. Transition Matrix Analysis

The complete 5×5 transition matrix (**Table 7**) quantified pixel-wise pathways of landscape transformation between 2022 and 2024. The most prominent off-diagonal transition was vegetation-to-built-up at 899.64 hectares, equivalent to 71.5% of the total 2024 built-up area and confirming direct forest-to-construction conversion as the dominant driver of built-up growth.

Table 7.

Transition matrix between 2022 and 2024 land cover classes (hectares).

From / To	Built-up	Bare	Vegetation	Cropland	Water	Total 2022
Built-up	276.57	63.48	369.55	75.74	0.01	785.35
Bare land	39.28	63.54	16.54	18.10	13.86	151.32
Vegetation	899.64	532.33	12,876.30	860.96	6.22	15,175.45
Cropland	43.35	45.89	233.84	286.64	20.76	630.48
Water	0.00	11.80	19.17	13.52	812.15	856.65
Total 2024	**1,258.83**	**717.06**	**13,515.40**	**1,254.96**	**852.99**	**17,599.25**

The vegetation-to-bare-land pathway (532.33 ha) represents a secondary clearing route, while bare-to-built-up transitions reached 39.28 hectares and cropland contributed 43.35 hectares to new built-up area. The diagonal entry for vegetation-to-vegetation (12,876.30 ha) confirms that the majority of forested cover remained intact despite concentrated transformation in the central KIPP zone.

Fig. 4 visualizes the transition matrix as a heatmap with logarithmic scaling to accommodate the wide range of transition magnitudes (from ~0.01 to 12,876 hectares). The diagonal cells (stable land covers) and the highlighted Vegetation→Built-up cell (899.64 ha, blue outline) represent the two most prominent patterns of landscape behavior during the 2022-2024 period.

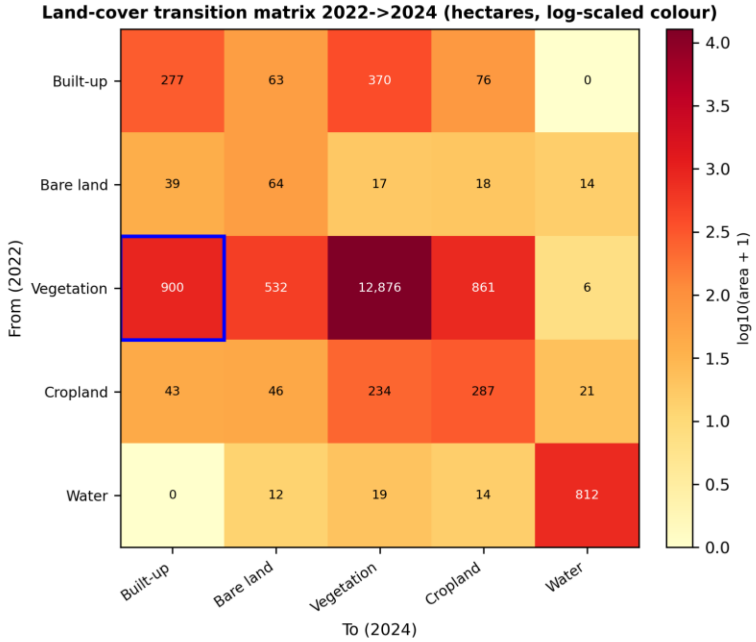

Fig. 4. Heatmap visualization of the 5×5 land cover transition matrix between 2022 and 2024 (hectares, log-scale).

3.4.1. Verification of Detected Changes

To provide reference-independent evidence for the detected transitions, a stratified random sample of 150 points (50 each on vegetation-to-built-up, built-up-to-vegetation and vegetation-to-bare-land) was cross-checked against Dynamic World a 10 m deep-learning land-cover product independent of both ESA WorldCover and the Random Forest classifier using annual modal labels for 2022 and 2024, and inspected on Sentinel-2 true-colour composites (**Fig. 5**). All 100 vegetation-origin points were vegetation in 2022 in Dynamic World, and 72% had left tree canopy by 2024; for the vegetation-to-built-up class specifically, 48% were labelled built-up or bare in Dynamic World for 2024, the remainder retaining a canopy label at mixed construction-edge pixels where the true-colour imagery nonetheless shows clearing (**Fig. 5**).

The built-up-to-vegetation anomaly was independently confirmed as commission error: none of its 50 points was built-up in Dynamic World in either year, so this class (369.55 ha) is a classification artefact rather than genuine revegetation and is excluded from the change total; the corrected area of significant change is 1,560.49 ha (8.9% of the ROI; Table 8). Google Open Buildings Temporal was also examined but does not yet register the IKN construction (building presence < 0.15 at its mid-2023 epoch) and was not used.

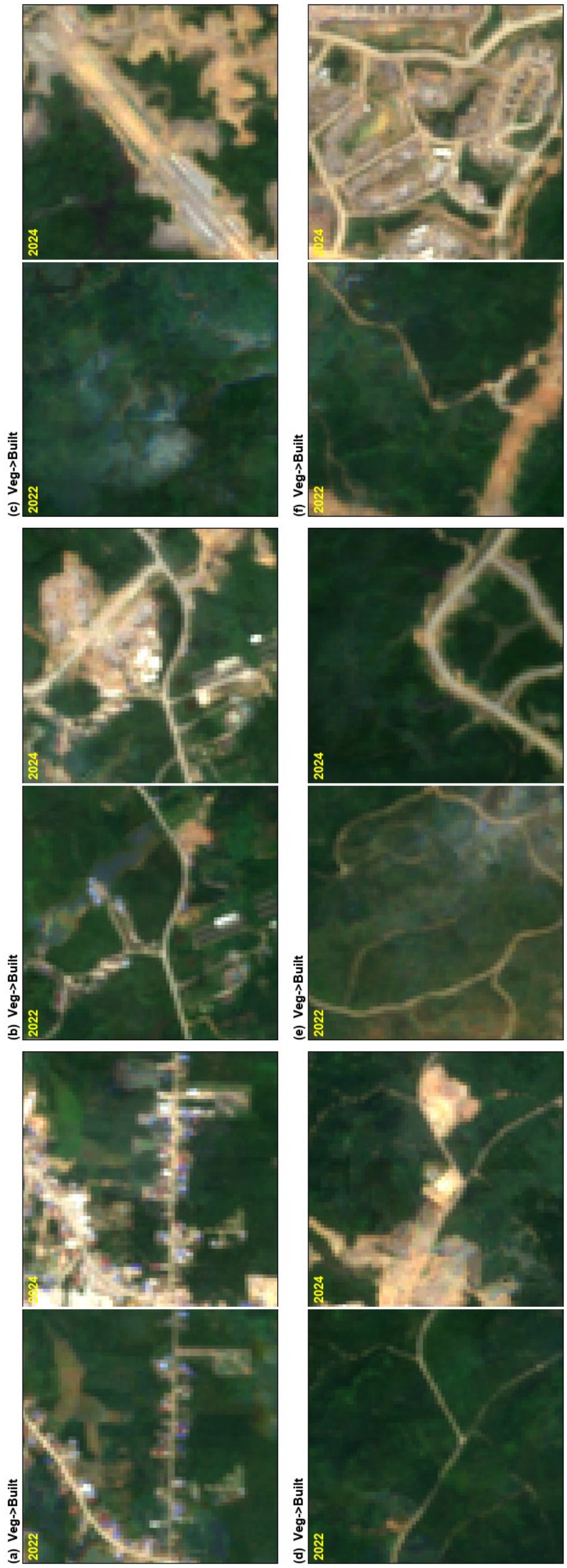

Fig. 5. Reference-independent verification (Section 3.4.1): Sentinel-2 true-colour composites for 2022 (left) and 2024 (right) at six representative vegetation-to-built-up sample points, each showing forest in 2022 and cleared or built ground in 2024.

3.5. Critical Land Cover Change Categories for GEOINT

Translation of the transition matrix into geospatial intelligence categories produced five critical change types plus one class (built-up-to-vegetation) excluded as commission error (**Table 8**). After that exclusion, confirmed by an independent Dynamic World check (Section 3.4.1), the total area of significant change is 1,560.49 hectares (8.9% of the ROI). The largest critical category was vegetation-to-built-up (899.64 ha, 5.1% of ROI) representing direct deforestation for construction, followed by vegetation-to-bare-land (532.33 ha, 3.0%) representing pre-construction land clearing. The combined critical built-up acquisition pathways (Veg→Built + Bare→Built + Crop→Built = 982.27 ha) directly support GEOINT operations including spatial planning verification and security perimeter monitoring.

Table 8.

Critical land cover change categories between 2022–2024.

Category	Description	Area (ha)	% ROI	GEOINT Significance
Veg → Built	Direct deforestation	899.64	5.1%	Critical (rapid impact)
Bare → Built	Construction completion	39.28	0.2%	High (planned)
Crop → Built	Agricultural conversion	43.35	0.2%	Moderate
Veg → Bare	Land clearing pipeline	532.33	3.0%	Future construction signal
Crop → Bare	Cropland clearing	45.89	0.3%	Low
Built → Veg (excluded)	Commission error, confirmed by Dynamic World (Sec. 3.4.1)	369.55	2.1%	not counted
Total significant change	**Sum of the five categories above**	**1,560.49**	**8.9%**	–

The spatial distribution of these critical change categories is visualized in **Fig. 6**, revealing distinct geographic patterns of transformation across KIPP IKN. The dark red areas (Veg→Built, critical) cluster predominantly in the central portion of the study area, corresponding to the core IKN development zone, while the orange Veg→Bare pattern (pre-construction pipeline) extends radially outward, indicating the spatial trajectory of future expansion.

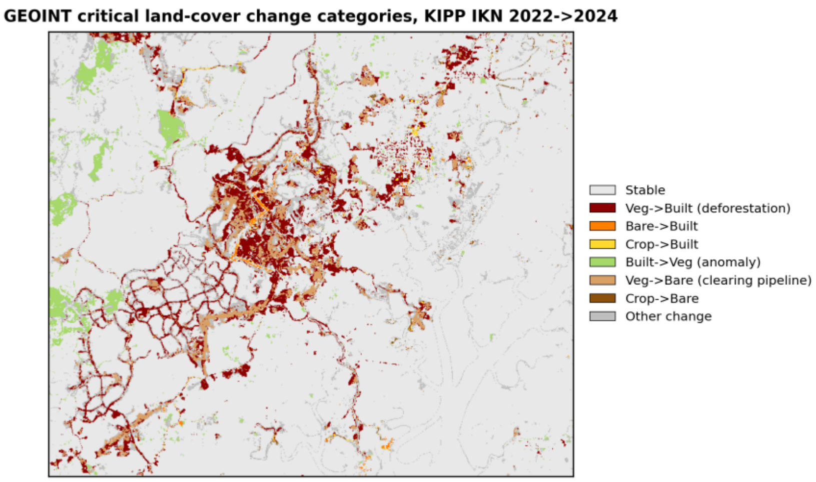

Fig. 6. GEOINT change category map of KIPP IKN 2022→2024, identifying six mapped transition types; with the built-up-to-vegetation class excluded as commission error (Section 3.4.1), total significant change is 1,560.49 ha (8.9% of ROI).

4. DISCUSSION

4.1. SAR-Optical Fusion Performance in Tropical Cloud-Affected Regions

The RF Fusion approach achieved 88.89% OA and 0.8609 Kappa for 2022, outperforming SAR-only (63.20%) and optical-only (86.44%). The 25.69-point gain over SAR-only confirms that complementary sensor information enhances classification under difficult atmospheric conditions, while the 2.45-point gain over optical-only reflects the marginal but consistent value of SAR integration in cloud-prone tropics. This aligns with prior tropical fusion studies: (Monsalve-Tellez et al., 2022) reported 82.14% OA in tropical Colombia (7.85 points over optical-only, 11.66 over SAR-only), a hierarchy remarkably similar to ours, supporting the generalizability of fusion beyond temperate settings. Recent Sentinel-1/2 fusion in Kuala Selangor, Malaysia-an analogous tropical Southeast Asian setting-similarly reported substantial benefits despite persistent cloud cover reducing optical continuity to fewer than 30 annual scenes (Jia et al., 2025). On the class-balanced test set the overall accuracy is the mean of the five per-class accuracies, so the small aggregate gain reflects averaging one large improvement against near-flat classes: the fusion benefit falls on built-up (+6.7 pp Producer's Accuracy, 2022) and cropland (+7.1 pp, 2024) the transition classes central to GEOINT monitoring (**Table 4**) while vegetation and water are already near-ceiling with the optical indices.

Importantly, the 2024 fusion result (85.12% OA, kappa=0.8127) maintained the performance hierarchy despite the transforming landscape, indicating that fusion robustness extends to non-stationary conditions-a critical property for operational monitoring during active construction. The 3.77-point decline from 2022 to 2024 primarily reflects temporal label-data mismatch (2021 labels versus 2022-2024 test data) rather than methodological weakness. Transformer-based fusion architectures could further improve accuracy by adaptively weighting sensors by local data reliability (Liu et al., 2024).

4.2. Built-up Expansion as GEOINT Indicator for IKN Development

The 60.3% expansion of built-up area (785.35 -> 1,258.83 ha) far exceeds typical urbanization rates for established Indonesian cities, placing KIPP IKN among the most rapidly transforming strategic zones globally (Purnama & Karondia, 2026). Critically, 71.5% of the 2024 built-up total originated directly from vegetation (899.64 ha Veg->Built), indicating an aggressive parallel-track approach where forest clearing and foundation work occur within compressed timeframes rather than the conventional clear-then-build sequence-a distinctive GEOINT signature of megaproject execution, with implications for environmental-impact and biodiversity-loss accounting. This extends the IKN-area characterization of (Habibie et al., 2025), who reported a forest-to-grassland shift across East Kalimantan; our short-interval, high-resolution approach reveals construction dynamics at a granularity not previously documented for KIPP. The vegetation-to-bare-land transition (532.33 ha), now secondary to the dominant Veg->Built pathway, remains a predictive signal for continued expansion through 2025-2026, supporting spatial planning and security-perimeter monitoring before construction completion. An independent cross-check against Dynamic World (150 stratified points) confirms that all sampled vegetation-to-built-up points were vegetated in 2022 and that 72% of vegetation-origin points had left tree canopy by 2024 (Section 3.4.1); the built-up-to-vegetation anomaly is confirmed as commission error and is excluded from the corrected significant-change total (1,560.49 ha, 8.9% of the ROI).

4.3. Limitations and Future Work

Several limitations warrant acknowledgment. First, training and reference labels derive from ESA WorldCover 2021 pseudo-labels rather than field-validated ground truth. For 2022 the one-year offset is minor; for 2024 the three-year offset adds label noise that both degrades training for the rapidly changing built-up and bare-land classes and shifts the accuracy reference away from 2024 ground truth (Section 2.7). Manually annotated or higher-resolution reference data would improve reliability. Second, the built-up-to-vegetation anomaly (369.55 ha) points to classification errors during construction transitions, where partially cleared areas, foundations, and exposed soil within single 10-m pixels create spectral ambiguity (Purnama & Karondia, 2026); an independent Dynamic

World check (Section 3.4.1) found none of a 50-point sample of this class to be built-up in either year, confirming it as commission error. Multi-temporal fusion across phenological cycles is promising: (H. Li et al., 2026) showed that integrating spectral, structural, and phenological attributes from Sentinel-1/2 time series improves accuracy in subtropical cloud-prone regions. Third, future work should incorporate ground-truthing of change hotspots, evaluate Sentinel-3 thermal data for urban heat-island assessment, and develop automated comparison against the official KIPP spatial plan.

5. CONCLUSIONS

This study developed and validated a cloud-based SAR-optical fusion framework using Random Forest for GEOINT monitoring of the KIPP of IKN Nusantara. Implemented in Google Earth Engine, it integrated 70 Sentinel-1 and 52 Sentinel-2 images for 2022 and 61 and 81 for 2024, across the 17,599-ha cloud-prone study area.

The RF Fusion approach achieved 88.89% OA and 0.8609 Kappa for 2022 (2.45 points over optical-only, significant at McNemar p=0.028; 25.69 points over SAR-only) and maintained the hierarchy for 2024 (85.12% OA, 0.8127 Kappa). Change detection revealed built-up expansion of 60.3% (785.35 -> 1,258.83 ha), of which 71.5% came directly from vegetation (899.64 ha Veg->Built)-a distinctive GEOINT signature of accelerated megaproject construction. The accompanying surge in bare land (+373.9%) and the 532.33-ha vegetation-to-bare-land transition together provide a predictive indicator for continued expansion through 2025-2026.

The novelty lies in integrating cloud-based SAR-optical fusion with short-interval (2-year) change detection calibrated for tropical megaproject monitoring, providing operational GEOINT capability for strategic infrastructure. Its reproducibility in Google Earth Engine supports scaling to the broader 256,000-ha IKN extent. Future work should add manually validated samples, deep-learning architectures, and automated comparison against the official KIPP spatial plan.

ACKNOWLEDGEMENTS

The authors thank the providers of the openly available datasets used in this study (Sentinel-1, Sentinel-2, and ESA WorldCover) and Google Earth Engine for cloud processing. The authors declare no conflict of interest. This research received no external funding. Reproducible Google Earth Engine code is available from the corresponding author on request.

REFERENCES

Adi, W.B., Anshar, A. & Muladi, A. (2025) Analisis Persebaran Zona Potensi Kawasan Rawan Kebakaran Hutan dan Lahan di Kecamatan Sambelia Menggunakan Metode Penginderaan Jauh dan Analisis Spasial. Jurnal Geosains Dan Remote Sensing, 6(1), 15–34. https://doi.org/10.23960/jgrs.ft.unila.382

Al-Dousari, A.E., Mishra, A. & Singh, S. (2023) Land use land cover change detection and urban sprawl prediction for Kuwait metropolitan region, using multi-layer perceptron neural networks (MLPNN). Egyptian Journal of Remote Sensing and Space Science, 26(2), 381–392. https://doi.org/10.1016/j.ejrs.2023.05.003

Aos, A.N.A. & Putri, N. (2023) Dinamika Vegetasi dan Suhu Permukaan Lahan Berbasis Remote Sensing di Waduk Jatigede Provinsi Jawa Barat: Studi Pendahuluan. Jurnal Geosains Dan Remote Sensing, 4(2), 67–76. https://doi.org/10.23960/jgrs.ft.unila.112

Carneiro, G.A., Svoboda, J., Cunha, A., Sousa, J.J. & Štych, P. (2025) Efficient 3D convolutional neural networks for Sentinel-2 land cover classification with limited ground truth data. European Journal of Remote Sensing, 58(1). https://doi.org/10.1080/22797254.2025.2512531

Cholidah Nina Nila Ziyana & Irawan Listyo Yudha. (2024) Pemanfaatan Penginderaan Jauh Untuk Pemetaan Alih Fungsi Lahan Sawah di Kabupaten Nganjuk. Jurnal Geosains Dan Remote Sensing. https://doi.org/10.23960/jgrs.ft.unila.203

Dagne, S.S., Hirpha, H.H., Tekoye, A.T., Dessie, Y.B. & Endeshaw, A.A. (2023) Fusion of sentinel-1 SAR and sentinel-2 MSI data for accurate Urban land use-land cover classification in Gondar City, Ethiopia. Environmental Systems Research, 12(1). https://doi.org/10.1186/s40068-023-00324-5

Djati, W.H. & Gunawan, D.S. (2025) Utilization Of Geospatial Intelligence (Geoint) In The Intelligence Cycle To Support The Role Of State Intelligence In Indonesia. Security Intelligence Terrorism Journal (SITJ), 2(3), 290–296. https://doi.org/10.70710/sitj.v2i3.65

Feng, X., Li, P. & Cheng, T. (2021) Detection of Urban Built-Up Area Change from Sentinel-2 Images Using Multiband Temporal Texture and One-Class Random Forest. IEEE Journal of Selected Topics in Applied Earth Observations and Remote Sensing, 14, 6974–6986. https://doi.org/10.1109/jstars.2021.3092064

Fitri, R., Fauzi, R., Seanders, O. & Danniswari, D. (2025) Land use changes and residential area expansion in South Tangerang City, Indonesia. Southeast Asia: A Multidisciplinary Journal, 25(2), 86–94. https://doi.org/10.1108/seamj-01-2023-0003

Gülci, S., Wing, M. & Akay, A.E. (2025) Land Use and Land Cover (LULC) Mapping Accuracy Using Single-Date Sentinel-2 MSI Imagery with Random Forest and Classification and Regression Tree Classifiers. Geomatics, 5(3). https://doi.org/10.3390/geomatics5030029

Habibie, M.I., Nurda, N., Fernando, D., Arifandri, R., Putra, P.K., Prayogi, H. & Sencaki, D.B. (2025) Integrating Sentinel-2 and ESA world cover for effective land use and land cover assessment using machine learning. Advances in Space Research, 76(9), 4925–4958. https://doi.org/10.1016/j.asr.2025.07.083

Irfan, A., Li, Y., E, X. & Sun, G. (2025) Land Use and Land Cover Classification with Deep Learning-Based Fusion of SAR and Optical Data. Remote Sensing, 17(7). https://doi.org/10.3390/rs17071298

Jagannathan, J., Vadivel, M.T. & Divya, C. (2025) Land use classification using multi-year Sentinel-2 images with deep learning ensemble network. Scientific Reports, 15(1). https://doi.org/10.1038/s41598-025-12512-7

Jia, P., Mohd Shafri, H.Z., Yu, S., Zheng, Z., You, S. & Mohamed Shariff, A.R. (2025) Radar-optical fusion of Sentinel-1/2 for high-resolution NDVI reconstruction and landscape-driven carbon flux assessment in Kuala Selangor, Malaysia (2020–2024). International Journal of Applied Earth Observation and Geoinformation, 145. https://doi.org/10.1016/j.jag.2025.104966

Jocea, A.F., Porumb, L., Necula, L. & Raducanu, D. (2025) Sentinel-2 Land Cover Classification: State-of-the-Art Methods and the Reality of Operational Deployment https://doi.org/10.3390/su172210324 A Systematic Review. In Sustainability (Switzerland) (Vol. 17, Number 22). Multidisciplinary Digital Publishing Institute (MDPI).

Kasahun, M. & Legesse, A. (2024) Machine learning for urban land use/ cover mapping: Comparison of artificial neural network, random forest and support vector machine, a case study of Dilla town. Heliyon, 10(20). https://doi.org/10.1016/j.heliyon.2024.e39146

Latif, R.M.A., Arshad, A., He, J., Ahmad, T. & Ahmed, A. (2025) Geospatial modeling and forecasting of urban land use change using Google Earth Engine and machine learning. PLOS ONE, 20(12 December). https://doi.org/10.1371/journal.pone.0338920

Lemenkova, P. (2025) Machine Learning Algorithms of Remote Sensing Data Processing for Mapping Changes in Land Cover Types over Central Apennines, Italy. Journal of Imaging, 11(5). https://doi.org/10.3390/jimaging11050153

Li, H., Luo, C., Kang, X., Luan, H. & Li, L. (2026) Multi-Temporal Fusion of Sentinel-1 and Sentinel-2 Data for High-Accuracy Tree Species Identification in Subtropical Regions. Remote Sensing, 18(4). https://doi.org/10.3390/rs18040592

Li, Y. & Xiao, X. (2025) Deep Learning-Based Fusion of Optical, Radar, and LiDAR Data for Advancing Land Monitoring. In Sensors (Vol. 25, Number 16). Multidisciplinary Digital Publishing Institute (MDPI). https://doi.org/10.3390/s25164991

Liu, R., Ling, J. & Zhang, H. (2024) SoftFormer: SAR-optical fusion transformer for urban land use and land cover classification. ISPRS Journal of Photogrammetry and Remote Sensing, 218, 277–293. https://doi.org/10.1016/j.isprsjprs.2024.09.012

Monsalve-tellez, J.M., Torres-león, J.L. & Garcés-gómez, Y.A. (2022) Evaluation of SAR and Optical Image Fusion Methods in Oil Palm Crop Cover Classification Using the Random Forest Algorithm. Agriculture (Switzerland), 12(7). https://doi.org/10.3390/agriculture12070955

Nigar, A., Li, Y., Jat Baloch, M.Y., Alrefaei, A.F. & Almutairi, M.H. (2024) Comparison of machine and deep learning algorithms using Google Earth Engine and Python for land classifications. Frontiers in Environmental Science, 12. https://doi.org/10.3389/fenvs.2024.1378443

Pande, C.B., Srivastava, A., Moharir, K.N., Radwan, N., Mohd Sidek, L., Alshehri, F., Pal, S.C., Tolche, A.D. & Zhran, M. (2024) Characterizing land use/land cover change dynamics by an enhanced random forest machine learning model: a Google Earth Engine implementation. Environmental Sciences Europe, 36(1). https://doi.org/10.1186/s12302-024-00901-0

Purnama, S.M. & Karondia, L.A. (2026) Utilizing Remote Sensing for Land Change and Night Lights in Urbanization: Correlation between Built-Up Area Expansion in Berau City and Changes in Climate Parameters. Geomatics and Environmental Engineering, 20(1), 93–115. https://doi.org/10.7494/geom.2026.20.1.93

Rangel, A., Terven, J., Córdova-Esparza, D.M., Romero-González, J.A., Ramírez-Pedraza, A., Chávez-Urbiola, E.A., Willars-Rodríguez, F.J. & Alfonso-Francia, G. (2025) Tracking U.S. Land Cover Changes: A Dataset of Sentinel-2 Imagery and Dynamic World Labels (2016–2024). Data, 10(5). https://doi.org/10.3390/data10050067

Septianto Aldiansyah, Randi Adrian Saputra, Khalil Abdul Wahid, Ilyas Madani & Duwi Setiyo. (2024) Rapid Flood Inundation Mapping Using Multi-Temporal Sentinel-1 SAR: An Example from Kendari City. Jurnal Geosains Dan Remote Sensing. https://doi.org/10.23960/jgrs.ft.unila.205

Shandu, I.D., Xulu, S. & Gebreslasie, M. (2026) Enhancing land cover classification in the heterogeneous landscape by integrating auxiliary data with Sentinel-2 imagery using the random forest algorithm. Frontiers in Remote Sensing, 6. https://doi.org/10.3389/frsen.2025.1697897

Syaban, A.S.N. & Appiah-Opoku, S. (2024) Unveiling the Complexities of Land Use Transition in Indonesia's New Capital City IKN Nusantara: A Multidimensional Conflict Analysis. Land, 13(5). https://doi.org/10.3390/land13050606

Yusfan, M.A., Supriyadi, A.A., Martha, S., Agus, R., Gultom, G. & Kartika Sakti, S. (2021) Geospatial Intelligence (GEOINT) As A National Defense Strategy for Information Overload in Indonesia. International Journal of Engineering, 3(2). https://doi.org/10.46923/ijets.v3i2.129

Yusuf Samad, M., Persadha, P., Ayu Permatasari, D., Adang Supriyadi, A., Prihanto, Y. & Dhae Ue, E. (2023) Analisis Intelijen Terhadap Manfaat Penginderaan Jauh dalam Memahami Aksi Kelompok Separatis di Indonesia Guna Mendukung Sistem Pertahanan Negara Intelligence Analysis of the Benefits of Remote Sensing in Understanding the Actions of Separatist Groups in Indonesia to Support the National Defense System Article info. 1, 55–74.